Lawrence Berkeley National Laboratory
LBL Publications

Title
Effects of Combustor Geometry on the Flowfields and Flame Properties of Low-Swirl Injector

Permalink
https://escholarship.org/uc/item/1856j6s5

Authors
Cheng, R.K.
Littlejohn, D.

Publication Date
2008-03-19

GT2008-50504

EFFECTS OF COMBUSTOR GEOMETRY ON THE
FLOWFIELDS AND FLAME PROPERTIES OF A LOW-SWIRL INJECTOR

R. K. Cheng and D. Littlejohn
Environmental Energy Technologies Div.
Lawrence Berkeley National Laboratory
Berkeley, CA 94720

ABSTRACT

The Low-swirl injector (LSI) is a novel dry-low NOx combustion method that is being developed for gas turbines to burn a variety of gaseous fuels including natural gas, low-Btu fuels, syngases and hydrogen. Its basic principle is described by a top level analytical model that relates the flame position to the flowfield similarity parameters and the turbulent flame speed correlation. The model was based on experimental measurements in open laboratory flames. It has been useful for guiding hardware development. As the LSI is being adapted to different engine configurations, one open question is how the combustor geometry and size affect its basic operating principle. The objective of this paper is to investigate these effects by conducting Particle Image Velocimetry (PIV) measurements in open and enclosed flames produced by a 6.35 cm diameter LSI using two quartz cylinders of 15.5 and 20 cm diameter to simulate the combustor casing. Results from 18 methane-air flames show that the enclosures do not alter the flame properties or the nearfield flow structures. The differences occur mostly in the farfield where the tighter enclosure deters the formation of a weak recirculation zone. The enclosure effects on hydrogen and hydrogen-methane flames were studies using the 20 cm cylinder. The results show that the outer recirculation zone generated at the corner of the dump plane promotes the formation of attached flames. However, the properties and nearfield flow features of the attached flames are similar to those of the lifted flames. At higher stoichiometries, the attached flame collapses to form a compact disc shaped flame that has very different flowfield structures. These results show that the enclosure effects on the LSI are strongly coupled to the fuel type and dump plane geometry but are less dependent on the enclosure size. These observations will provide the basis for developing computational methods that can be used as design tools for LSI adaptation.

INTRODUCTION

Our research is motivated by the need of a cost effective, robust, and ultra-low emission combustor for the gas turbines in FutureGen power plant that burns syngases derived from gasification of coal. The objective is to adapt the low-swirl combustion method to these utility size gas turbines that operate on fuels with very high H_2 constituency. Low-swirl combustion is a dry-low-NO_x lean premixed combustion method that has been commercialized for industrial heaters. Low-swirl injectors (LSI) have been developed for natural gas industrial turbines (5 – 7 MW) in partnership with Solar Turbines of San Diego, California, and for microturbines (100 kW) in partnership with Elliott Energy Systems of Stuart, Florida [1, 2].

The FutureGen power plant utilizes the Integrated Gasification Combined Cycle (IGCC) approach to produce hydrogen, which is separated from a concentrated CO_2 stream that is then captured for subsequent sequestration. One of its key components is a cost-competitive all-hydrogen fueled turbine with ultra low NO_x emission and high efficiency. To lower NO_x to the FutureGen near zero emission goal of 2 ppm (@ 15% O_2), the current approach is to operate the H_2 turbine at lower firing temperatures in combination with selective catalytic reduction. This approach sacrifices efficiency and impacts costs of electricity (via capital cost, efficiency and capacity output). Therefore, a cost-effective combustion technology that meets the FurtureGen emissions and efficiency targets is critical to achieving its ultimate goal of no more than a 10% increase in cost of electricity for mature FutureGen type plants that include CO_2 capture and sequestration.

To investigate the feasibility of the low-swirl combustion concept for IGCC turbines, our previous studies reported laboratory experiments that provided some preliminary information to guide its adaptation to burn pure H_2 and syngases [3]. The velocity data obtained from particle image velocimetry (PIV) showed that the overall flowfield features of the H_2 flames are not significantly different from those of the hydrocarbon flames. The turbulent flame speeds of the H_2 flames correlate linearly with turbulence intensity, u'. The value of the turbulent flame speed correlation constant of 3.1 is about 50% higher than the value of 2.14 determined for the hydrocarbon flames. Comparison of the mean and rms velocity profiles show that the nearfields of the H_2 flames exhibit self-similarity features that are similar to those found in hydrocarbon flames. Therefore, the LSI mechanism is not sensitive to the differences in the hydrocarbons and H_2 flame properties. Therefore, the LSI concept is amenable to burning of H_2 fuels.

The overwhelming majority of our previous laboratory studies were conducted in open flames to facilitate the collection of a large amount of high-fidelity experimental data from laser diagnostics suitable for detailed analysis. There is only one set of data of enclosed flames collected at a very low velocity of U_0 = 3 m/s [4]. The study showed that the enclosure effects are minimal when the enclosure radius is about three times larger than the injector (or burner) radius. The 3:1 enclosure ratio has been adopted as the guideline for sizing the enclosures for industrial burners and for optimizing the LSI radius for the gas turbine combustor [1]. Because the 3:1 rule seems to be valid for both atmospheric and gas turbine applications, the effects of enclosures on the quantitative features of the LSI flowfields especially at higher flow velocities have yet to be explored. However, to scale the LSI to the large utility turbines, the use of CFD is a necessary design tool. But there is insufficient knowledge on the enclosed LSI flame and flowfield to evaluate the CFD results. The purpose of this paper is to investigate and analyze the enclosure effects on hydrocarbon and H_2 flames to gain the knowledge for guiding the development of robust CFD for LSI development.

NOMENCLATURE

$a_x = \dfrac{dU/dx}{U_0}$ normalized axial flow divergence (1/mm)

$a_r = \dfrac{dV/dr}{U_0}$ normalized radial flow divergence (1/mm)

D   diameter of the LSI, 6.35 cm
L_i swirler recess distance
$m = m_c/m_s$ mass flux ratio through LSI
m_c mass flux through center channel
m_s mass flux through swirl annulus
M_0 total mass flux through the LSI
M_r recirculated mass flux
q'   2D turbulent kinetic energy = $\frac{1}{2}(u'^2+v'^2)^{1/2}$

Re   Reynolds number $2R_iU_0/\nu$
$R = R_c/R_i$ ratio of the center channel radius, R_c to injector radius, R_i
r   radial distance
S   swirl number
S_L laminar flame speed
S_T turbulent flame speed
T_{ad} adiabatic flame temperature
U_0 bulk flow velocity
U   axial velocity
u'   axial rms velocity
v'   radial rms velocity
uv   shear stress
x   axial distance from injector exit
x_f leading edge position of the flame brush
x_o virtual origin of divergent flow

BACKGROUND

The LSI is based on an aerodynamic flame stabilization method that utilizes a divergent flow to sustain a freely propagating premixed turbulent flame[5]. The divergent flow is formed only when the swirl intensities are well below the critical vortex breakdown threshold. Linear decay of the axial velocity within the divergent flow allows the flame to settle where the local velocity is equal and opposite to the turbulent flame speed. Matching the flowfield velocities to the turbulent flame speed is therefore the critical design criterion.
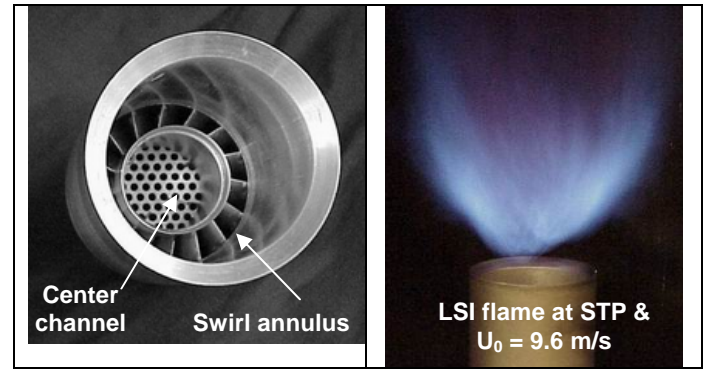

Fig. 1: The first prototype LSI for Taurus 70 engine

The key component of the LSI is a swirler that supplies the reactants through two passages: an outer annulus with swirl vanes and an open center-channel that allows a portion of the reactants to remain unswirled [6] (Fig. 1). The supply of unswirled reactants through its center is the unique feature of the LSI and its presence retards the formation of a central recirculation zone and promotes the formation of flow divergence. The flame is detached from the LSI. Its lift-off position is controlled by the divergence rate that can be adjusted by changing the flow split between the swirled and the unswirled flows. The most convenient means to change the flow split is by varying the blockage ratio of the perforated screen covering the center-channel.

The LSI of Fig 1 utilizes an annular vane swirler that has been developed for Solar Turbine's T70 SoLoNOx injector [1]. To convert the swirler from high-swirl to low-swirl operation, its center bluff body is removed and replaced by a perforated plate whose blockage ratio is selected to give a swirl number, S, within the range of 0.4 to 0.55. The swirl number is defined as

$$S = \frac{2}{3}\tan\alpha \frac{1-R^3}{1-R^2+[m^2(1/R^2-1)^2]R^2} \qquad \text{Eq. (1)}$$

where α is the vane angle and $R = R_c/R_i$. $m = m_c/m_s$ where m_c and m_s are respectively the mass fluxes of the unswirled and the swirled flows, and is inversely proportional to the blockage ratio of the perforated plate. The SoLoNOx swirler has an internal radius of 3.175 cm and consists of sixteen curved vanes with a discharge angle $\alpha = 40^o$. The center-channel to injector radius ratio R is 0.63. As reported previously, a perforated plate of 58% blockage with holes in a hexagonal arrangement renders a LSI with S = 0.54 that has shown to be operable for natural gas and other hydrocarbon fuels as well as various diluted hydrogen and hydrocarbon fuel blends. For hydrogen, the swirl number is relaxed to 0.5 and the use of a perforated plate with variable hole offers a flame shaping means to push out the LSI flame and deter the H_2 flame from attaching to the LSI rim [3].

The scientific foundation obtained for the LSI plays a central role for its adaptation to gas turbines (e.g. [7-12]. Analyses of the velocity measurements show that the LSI flowfield exhibits self-similarity behavior. Two parameters deduced from the centerline velocity profiles are invoked to characterize self-similar behavior [13, 14]. They are the virtual origin of the divergent flow, x_0, and the non-dimensional axial aerodynamic stretch rate, a_x. To characterize the flame, the turbulent flame speeds, S_T, and the position of the leading edge of the flame brush, x_f, are used. Analysis of S_T shows a linear dependency on turbulence intensity, u'. An analytical equation (Eq. 2) for the velocity balance at x_f, shows that a coupling of the self-similar flowfield and a linear turbulent flame speed correlations with u' is the reason why the LSI flame remains stationary through a wide range of velocities and fuel air equivalence ratios, ϕ.

$$1 - \frac{dU}{dx}\frac{(x_f - x_o)}{U_o} = \frac{S_T}{U_0} = \frac{S_L}{U_o} + \frac{K u'}{U_0} \qquad \text{Eq. (2)}$$

The two terms on the far RHS simply state that S_T for hydrocarbon flames increases linearly with u' above the baseline value of the laminar flame speed, S_L, at a slope of K. This slope is an empirical correlation constant derived from the experimental measurements[1] and is 2.16 for hydrocarbon flames and 3.1 for hydrogen flames. The first term of RHS tends to a small value at large bulk flow velocity U_0 because the laminar flame speeds of typical hydrocarbon and hydrogen

---

[1] Linear dependency of S_T on u' is not universal as S_T in other burners tends to be non-linear and shows "bending"

flames at the ultra-lean operating conditions of gas turbines are on the order of 0.2 to 0.3 m/s. The second term on RHS is a constant because turbulence in the LSI is controlled by the perforated plate and scales with U_0. On the left hand side, self-similar means that $a_x = dU/dx/U_o$ in the second term is constant. The main consequence is that for a given value of K the flame position $x_f - x_0$ has an asymptotic value at large U_0. Therefore, when S_L is held constant at a certain ϕ, significant flame shift, i.e. changes in x_f, occurs only at low velocities where U_0 is in the same order as S_L. When $U_0 >> S_L$, changing stoichiometry and/or U_0 do not generate significant flame shift. The effect of a high value of the turbulent flame speed correlation parameter, K, as for the pure hydrogen flames, is an upstream shift in the asymptotic flame position. These flame behaviors have been confirmed by laboratory experiments at atmospheric and simulated gas turbine conditions.

Eq. 2 is a simple linear analytical expression that describes the relationship between the LSI flowfield and the turbulent flame properties. Because the aerodynamic stretch rate is proportional to the swirl number, this expression is a convenient top order model to show how the LSI can be adjusted to accept different fuels. The goal of this study is to determine if this model needs to be adjusted to include the effects due to enclosures.

EXPERIMENTAL APPARATUS & DIAGNOSTICS

The LSI-VH1 with S = 0.51 employed in our previous study [3] is a logical choice for the evaluation of the enclosure effects because it offers the widest range of operation for H_2. It is 6.35 cm in diameter with a center-channel of 4 cm diameters. The swirler has sixteen curved vanes with $\alpha = 40^0$ and is recessed 9.5 cm from the exit. The center channel plate has variable hole sizes as shown in the insert of Fig. 2. It is mounted vertically on top of a cylindrical settling chamber (Fig. 2) with air supplied by a fan blower enters at its e side of and flows into the LSI via a centrally placed 30 cm long straight tube. To produce a uniform flow into the LSI, a perforated screen is placed 5 cm upstream. The air flow rate is adjusted by a PC controlled valve and monitored by a turbine meter. Fuel is injected into a commercial venturi premixer to ensure a supply of homogeneous mixture to the injector. Both the fuel and the PIV seeder flows are controlled by electronic mass flow controllers and set according to a predetermined value of mixture compositions and ϕ. The fuel and air supply system has a maximum capacity of 65 g/s to deliver maximum bulk flow velocity $U_0 = 22$ m/s.

Two 35 cm long quartz cylinders of 15.5 and 20 cm in diameter were used to simulate the combustor enclosure. The larger cylinder is identical to the one used at Solar Turbines for testing the LSI with preheated air at atmospheric pressure. It has an enclosure to LSI diameter ratio of 3.15. The smaller quartz cylinder offers a more restrictive enclosure ratio of 2.44 and is compatible with the silo combustor configuration of the Elliott microturbine. The quartz cylinders are mounted to the

LSI on planar circular flanges so that the LSI discharges into a sudden expansion (or step) dump plane at the entrance of the combustion chamber. The LSI protrudes about 5 cm beyond the dump plane to allow the PIV laser sheet to be placed as close as possible to the LSI exit. As in the Solar Turbine setup, there were no constrictions at the exit of the quartz cylinders.

Flowfield information was obtained using Particle Imaging Velocimetry (PIV). The PIV system consists of a New Wave Solo PIV laser with double 120 mJ pulses at 532 nm and a Kodak/Red Lake ES 4.0 digital camera with 2048 by 2048 pixel resolution. The optics captured a field of view of approximately 13 cm by 13 cm covering the nearfield as well as the farfield of the flames with 0.065 mm/pixel resolution. A cyclone type particle seeder seeds the air flow with 0.6-0.8 μm Al_2O_3 particles which should track velocity fluctuations up to 10kHz [15].

Data acquisition and analysis were performed using software developed by Wernet [16]. Because of the complex and 3D nature of the swirling flow-field, care had to be taken to optimize interframe timing, camera aperture setting, light-sheet thickness, and seed density to ensure high data fidelity. Using a portion of the light sheet with approximately 1.1 mm thickness (away from the 0.3 mm waist produced by the 450 mm spherical lens) and a short interframe time (25 μs) helped to freeze the out-of-plane motion of seed particles. Sets of 224 image pairs were recorded for each experiment corresponding

to minimum criterion required to produce stable mean and rms velocities. The PIV data were processed using 64x64 pixel cross-correlation interrogation regions with 25% overlap. This rendered a spatial resolution of approximately 2 mm. The velocity statistics were checked to ensure that significant spatial bias or "peak-locking" was not taking place.

The main difficulty in applying PIV to enclosed flows is the reflection of the laser light from the external and internal curved surfaces. As a result, data are not reliable from areas where the bright reflections overwhelm the Mie scattering signals. Deposition of the seed particles on the internal wall of the quartz cylinder is another phenomenon that degrades data quality. These problems can be addressed by careful positioning of laser beam blocks and spatial filters, and by frequent cleaning of the cylinders in between runs or by conducting multiple short runs to limit particle build-up. To a lesser extent, the optical aberration due to capturing the PIV image through the curved transparent wall also affects the accuracy of the radial velocity component. Because the quartz cylinder wall is thin (3.17 mm), at the side edges of the PIV domain, the uncertainties introduced by the refractivity on the radial positions of the velocity vectors and the radial velocity components are respectively < 1 mm and < 1%. As the velocity analysis is focus on the centerline profiles where the optical effects are the much less, no attempt was made to correct for the optical effects.
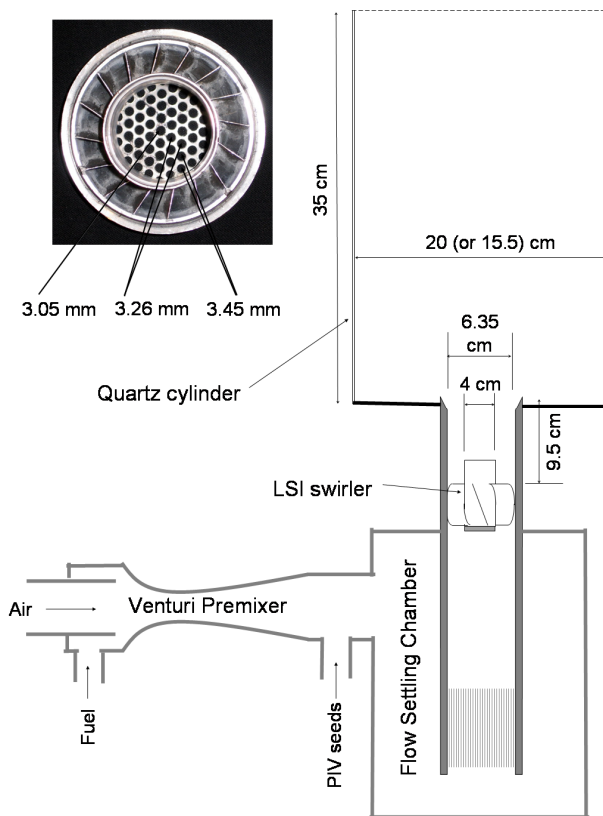
RESULTS

Table I shows the mixtures used in this study. To provide the necessary background, the non-reacting flowfields within the two enclosures were investigated at five velocities between $10 < U_0 < 18$ m/s and compared with the corresponding open flows. The flame experiments were conducted at $U_0 = 10$, 14 and 18 m/s. The CH_4-air flames were investigated in both enclosures while the H_2 and 0.75 H_2 / 0.25 CH_4 flames were studied only in the 20 cm enclosure. Though these velocities are lower than typical gas turbine operating velocities of 30 to 70 m/s, our previous studies [1, 2] that these laboratory flame experiments can provide the insights to guide the development of gas turbine hardware.

Table I - Mixtures for the open and enclosed flames

Fuel	ϕ	T_{ad} (K)	S_L (m/s)
CH_4	0.6	1669	0.115
CH_4	0.7	1849	0.2
H_2	0.35	1312	0.18
0.75 H_2 / 0.25 CH_4	0.45	1450	0.21
0.75 H_2 / 0.25 CH_4	0.5	1555	0.27

Non-Reacting Flows

Fig. 3 compares the open and enclosed non-reacting flowfields at $U_0 = 14$ m/s. It is quite obvious that the enclosures cause significant changes to the overall features of the flowfields. The most noticeable change, as outlined by the broken white line making the contour of zero mean axial
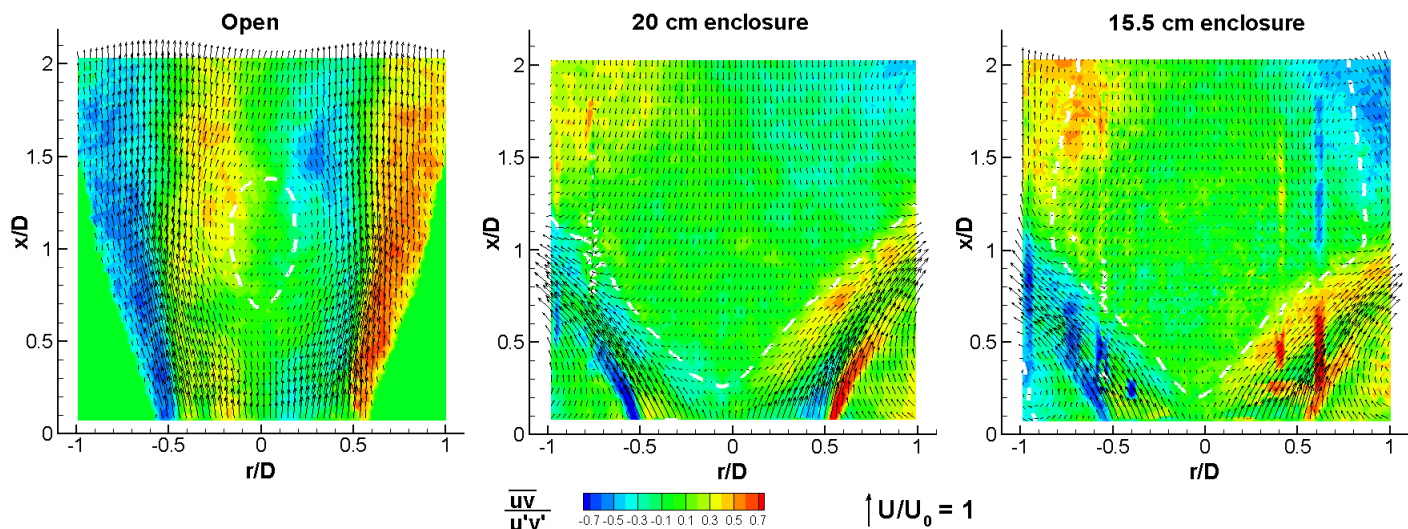

Fig 2 Schematics of the LSI setup

Fig 3 Normalized velocity vectors and Reynolds shear stress obtained for open and enclosed non-reacting flows at $U_0 = 14$ m/s

velocity U = 0, is the enlargement of the recirculation zone. In the open, the recirculation zone appears as a small bubble center at x/D = 1. The flow recovers downstream of the bubble and the velocity vectors leaving the PIV domain have positive axial velocities. These characteristics are typical of the open flows produced by other LSIs and low-swirl burners.

Within the 20 cm enclosure, the recirculation zone enlarges and covers more than half of the PIV domain. The upstream stagnation point of the recirculation zone moves very close to the LSI exit at x/D = 0.25. The U = 0 contour extends beyond the side boundaries to show that the recirculation zone is larger than the width of the PIV domain. The velocity vectors at the top of the PIV domain all have negative axial component to indicate a strong backflow. The discharge angle of the enclosed LSI flow being much larger than in the open flow is illustrated by the contours of large positive and negative Reynolds shear stresses and by the angles of the velocity vectors pointing outward from the PIV domain at 0.6 < x/D < 1. These changes in the non-reacting flowfield induced by the 20 cm enclosure are symptomatic of an over expanded flow. Due to its divergent nature, the LSI flow has a natural tendency to fill the enclosure volume. When the area ratio prescribed by enclosure is larger than the open flow's normal expansion ratio, the flow over expands to generate a stronger adverse axial mean pressure gradient and a large recirculation zone.

In the nearfield, the formation of an outer flow recirculation region is illustrated by the flow rotations shown at the lower left and right corners of the PIV domain. The outer recirculation is found in almost all enclosed swirling flows discharging into an enclosure with a sudden-expansion dump plane [17].

The general features of the non-reacting flow in the 15.5 cm are similar to those in the 20.0 cm enclosures. The upstream stagnation point occurs at a similar location and the flow discharge angle is not very different. Because the 15.5 cm enclosure is smaller, the PIV domain captured the flow outside of the center recirculation bubble where a fast flowing region adjacent to the cylinder wall is found.
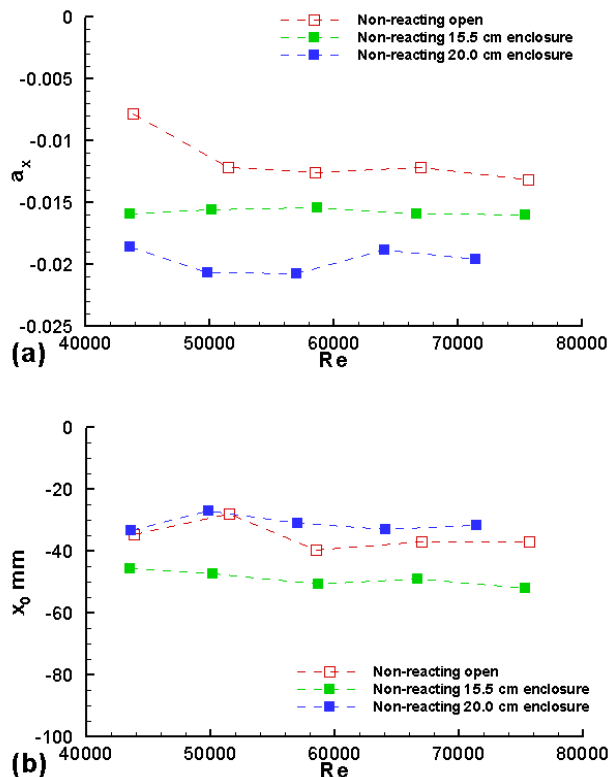

Fig 4 (a) Normalized axial divergence, a_x and (b) virtual origins of the non-reacting flows

5

The degradation of the PIV data due to reflections of the incident laser sheet from the 15.5 cm quartz enclosure are marked by the vertical streaks of intense $\overline{uv}/u'v'$ at r/D = ± 0.6. The degradation of the data obtained for the larger 20 cm enclosure are less discernable at r/D = ± 0.75 where they cause scatterings in the mean velocity vectors. These results show that the influence of laser light reflections appeared in well-defined and relatively small regions and they do not obscure the key LSI flowfield features near the centerline region where the velocity data are crucial to the analysis.

To examine the nearfield self-similarity features of the open and the enclosed non-reacting flows, the normalized axial divergence a_x and the virtual origin x_0 were deduced from the centerline velocity profiles according to the definitions and procedure described in Ref. [18]. The results are compared in Fig. 4. The a_x profiles (Fig. 4a) show that the normalized divergence rate increases with enclosure size and the trend is consistent with the explanation of the flow over-expanding to fill the enclosure. For all three cases, a_x is not sensitive to Re except for the open flow at low Re where a sudden decrease is shown above Re = 40,000. The virtual origins of the open and enclosed non-reacting flows are compared in Fig. 4b and show relatively flat x_0 distributions for all three cases. Enclosure effects on x_0, however, is found only for the case with the smaller 15.5 cm cylinder where the x_0 profile assumes lower

values to indicate an upstream shift of the divergent flow structure. The overall trends of a_x and x_0 in Fig 4 illustrate that the enclosed non-reacting LSI flowfields are also self-similar.

The self-similar features of the open and enclosed non-reacting flows are compared in Fig 5 by the normalized U/U_0 and q'/U_0 profiles deduced along the centerline. These axial profiles are plotted with respect to the virtual origin, x_0. Fig 5a shows that all except one of the U/U_0 profiles collapse onto their respective trends. The exception is the profile for the open flow at the lowest velocity $U_0 = 10$ m/s. Because the other four profiles at higher velocities are consistent, this shows that the open flow does not become fully developed until Re > 50000. In contrast, the two sets of profiles for the enclosed flows are self-consistent. Therefore, the enclosed flows become fully developed at lower Reynolds numbers.

For the two enclosed flows, steep linear decay of U/U_0 in the nearfield is accompanied by the upstream shift of the stagnation points of their recirculation zones (i.e. the zero crossing points). Downstream of the stagnation point, the U/U_0
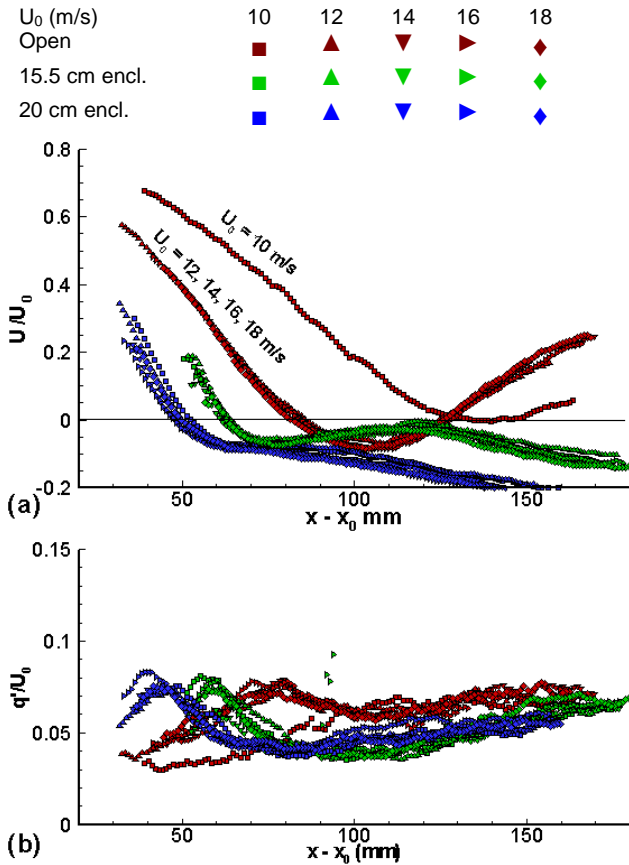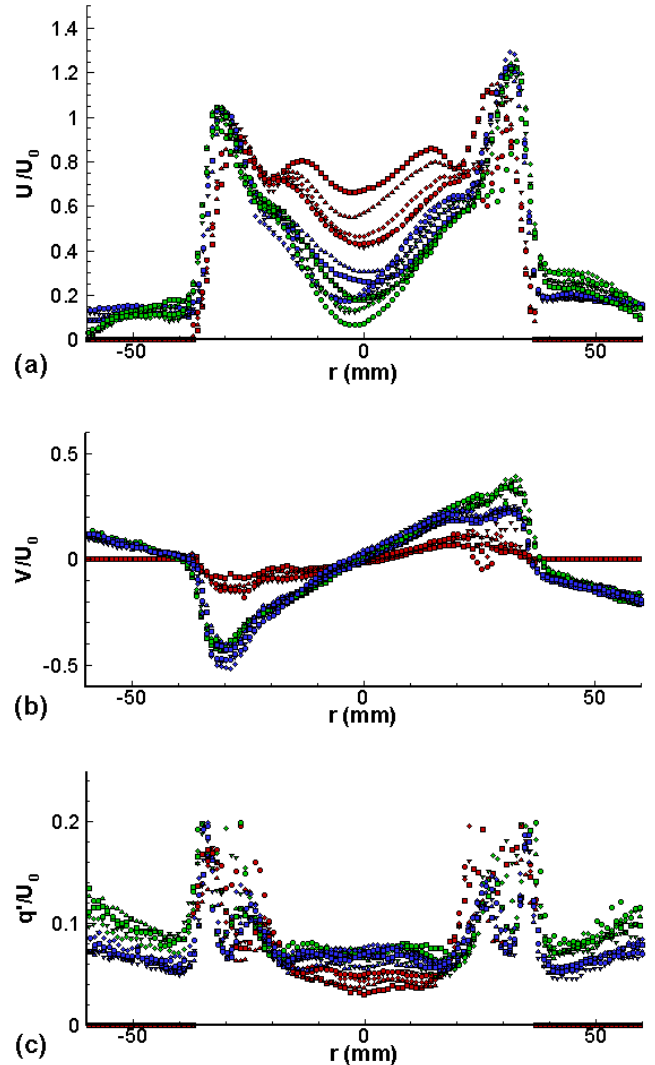

(a)

(b)

Fig 6 Radial profiles of open and enclosed non-reacting flows at x = 6.5 mm. Symbol legend same as Fig. 5.

Fig 5 Centerline profiles for open and non-reacting flows

6

profiles stay below zero and become more negative with increasing downstream distance. As shown by the corresponding q'/U_0 profiles (Fig. 5b), the turbulence kinetic energies are relatively insensitive to the enclosure effects. For all three sets of non-reacting flow data, q'/U_0 peaks near the stagnation point and the values at the peaks are about the same. Except for a slight drop in q'/U_0 below the stagnation points of the enclosed flows, the distributions of the turbulent kinetic energies in the recirculation zones are relatively flat.

The radial profiles of the non-reacting flows at x = 6.5 mm are compared in Fig. 6. The U/U_0 profiles in Fig 6a show that the enclosure effects are found mostly within the central region of -20 < r < 20 mm. Because this LSI was fitted with a perforated plate with varying hole sizes, a velocity deficit in the central region is a characteristic flowfield features. Within the central region, the open flow U/U_0 profiles are scattered due to its developing nature at the lower range of Re. The enclosed flow profiles are more consistent to show again that they are fully developed and self-similar. Using the minimum U/U_0 near r = 0 as a means of comparison, it can be seen that the enclosure causes a significant drop in U/U_0 compared to the open cases due to the increases in flow divergence.

The influence of the enclosures on flow divergence is also shown in Fig. 6b by the V/U_0 profiles where the slopes of the central linear V/U_0 regions of the enclosed flows are steeper slopes than the open flows. The normalized radial divergence a_r for the open flow is 0.006 mm^{-1} and is 0.012 mm^{-1} for the enclosed flows. From Fig 4 the corresponding a_x are respectively -0.0125, -0.016 and -0.019 for the open, 15.5 cm enclosed and 20 cm enclosed flows. The $a_x/a_r = 2$ ratio for the open flow is typical of the non-reacting LSI flowfields and is consistent with the a_x/a_r ratio for a stagnating flow against a flat plate. However, the a_x/a_r ratios for the enclosed flows are smaller and demonstrate that the enclosures and their side boundary conditions have altered the mean strain fields that

dominate the LSI flowfield development.

The radial q'/U_0 profiles in Fig 6c show that the distributions of the turbulent kinetic energy within the central region are relatively uniform despite the central deficit in U/U_0. The q'/U_0 levels measured in the enclosed flows are slightly higher than in the open flows. The increase can be attributed to the increases in the axial and radial strain rates.

Enclosed CH$_4$ flames

The flowfields of the open and enclosed CH$_4$-air flames at U_0 = 14 m/s with ϕ = 0.7 and 0.6 are shown respectively in Figs. 7 and 8. For these sets, data degradation of the enclosed flames are more severe than in the non-reacting cases due to the flame impinging on the cylinder wall and hastening seed particles build-up. Despite these difficulties, the nearfields of the enclosed flames are relatively free of the degradations to provide reasonable data for the analysis.

From Fig. 7, the most noticeable difference between the three flames is the presence of central downstream recirculation zones in the open and 20 cm enclosed flames and the absence of one in the 15.5 cm enclosure. Though the recirculation zone of the 20 cm enclosed flame is slightly off-center, its size is compatible with the one found in the open flame. In contrast, the farfield of the same flame enclosed in a slight smaller 15.5 cm cylinder is devoid of a central recirculation zone and the velocity vectors leaving the PIV domain are all positive. Despite the differences in the farfield the velocity vectors in the nearfields are not significantly different. Additionally, the discharge angles of the flow, as shown by the intense $\overline{uv}/u'v'$ regions, are consistent. For the two enclosed flames, the formation of the outer recirculation zone is also evident.

In Fig. 8, the general features and trends of the flowfields of the weaker ϕ = 0.6 flames are similar to those of the ϕ = 0.7 flames. Central recirculation zones are found in the open
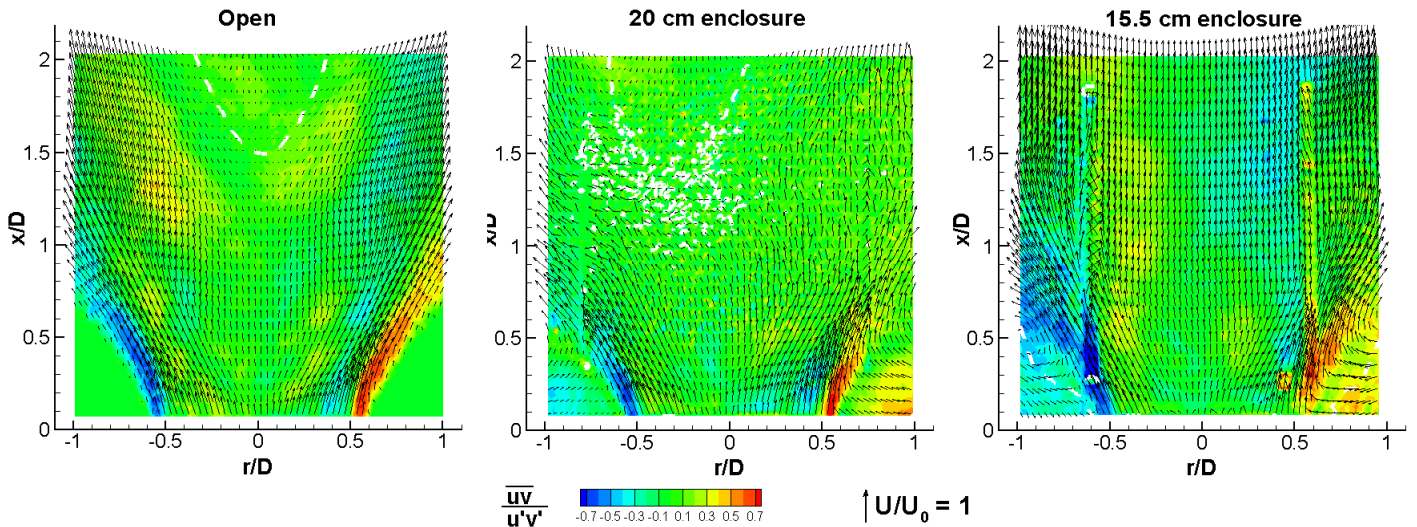

Fig 7 Normalized velocity vectors and Reynolds shear stress of open and enclosed CH$_4$/air flames at ϕ = 0.7 and U_0 = 14 m/s
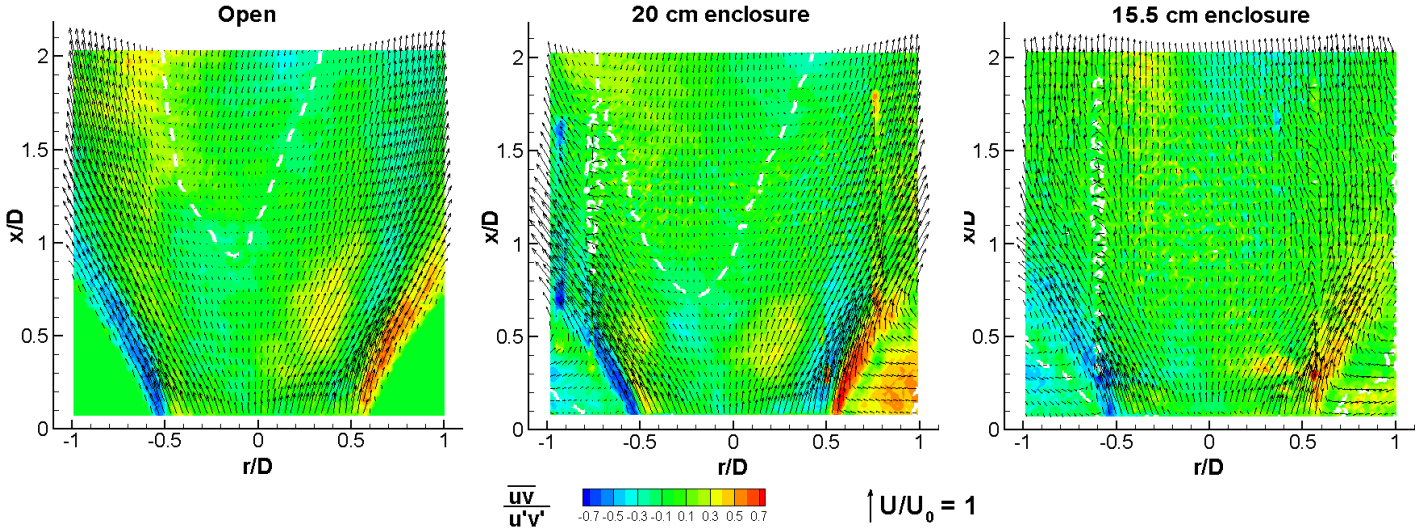
Fig 8 Normalized velocity vectors and Reynolds shear stress of open and enclosed CH_4/air flames at $\phi = 0.6$ and $U_0 = 14$ m/s

flames and in the 20.0 cm enclosed flames. They are larger than those formed in the $\phi = 0.7$ flames but their locations are compatible. Again, the central recirculation zone is not formed in the smaller 15.5 cm and the velocity vectors at the top edge of the PIV domains are all positive. In the nearfield, similarity of the flow discharge angles, the velocity vector distributions, and the formation of outer recirculation in the enclosed cases are all consistent with those found in Fig. 7.

To examine the nearfield self-similarity features of the open and enclosed CH_4 flame flowfields, the normalized divergence, a_x and virtual origin, x_0 deduced from the centerline U/U_0 profiles are shown in Fig. 9. Fig. 9a shows that a_x is not sensitive to the enclosure effects as they are nearly the same for the open and enclosed cases. At Re < 50,000, the $\phi = 0.6$ and 0.7 have different a_x values but the two sets of data converge at high Re to $a_x = -0.018$ mm^{-1}. The consistent trend is quite unlike the non-reacting flows results where the values of a_x vary with enclosure size. The highest value of $a_x = -0.02$ for the non-reacting flows in the 20 cm enclosure is closest to those found for all the flames. The results of x_0 in Fig 9b show again that the nearfields of the flames are not significantly affected by the enclosures. All x_0 scatter around -38 mm that is again consistent with the values obtained for the 20 cm enclosed non-reacting flows. The results shown in Fig 9 demonstrate that the nearfields of the enclosed flames are self-similar. The significant implication is that the enclosures do not alter the nearfield features of the reacting flows.

The centerline profiles of the open and enclosed flames are compared in Figs. 10 and 11. The U/U_0 profiles for the $\phi = 0.7$ flames in Fig. 10a show that the open flame at $U_0 = 10$ m/s has features that are different than the rest. Its U/U_0 value at the LSI exit is relatively high (0.6) and the flame is more lifted as indicated by the position (x - x_0 = 60 mm) of the local minimum following the initial linear U/U_0 decay. Disregarding this profile, the nearfield features of the other open flames and the enclosed flames are similar. They all have a small linear decay region in the near field followed by a slight acceleration due to heat release. For the open and the 20 cm enclosed cases, the U/U_0 profiles decrease in the post flame regions and drop below zero to show the formation of weak central recirculation zones. In contrast, profiles for the 15.5 cm enclosed flames show a continuous increasing trend in the farfield. The q'/U_0
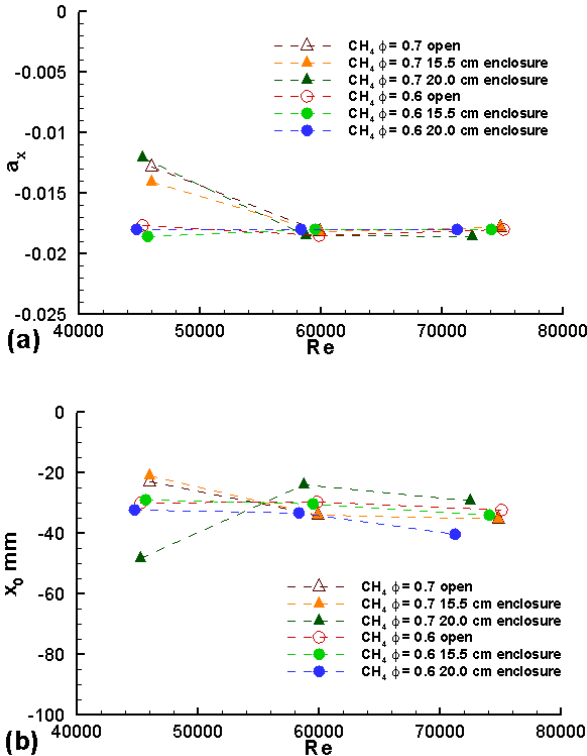

Fig 9 (a) normalized axial divergence, a_x and (b) virtual origins of open and enclosed CH_4/air flames
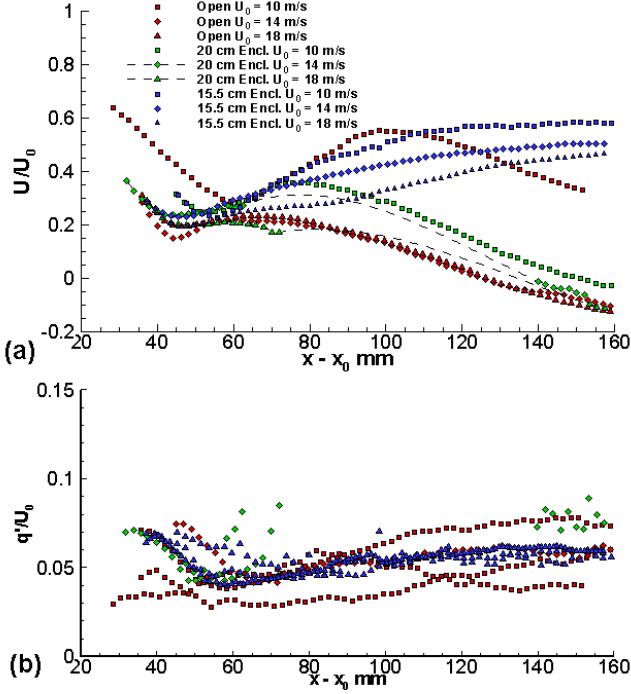
Fig 10 Axial profiles of open and enclosed $\phi = 0.7$ CH$_4$/air flames

Fig 11 Axial profiles of open and enclosed f = 0.6 CH$_4$/air

profiles in Fig. 10b are more scattered than those found in the open flames and it is a consequence of the degradation of the PIV image affecting the second moment statistics. Despite the scatter, the trends of these profiles are consistent regardless of the differences in the farfield flow structures.

In Fig. 11a, the open and enclosed flame U/U$_0$ profiles for the $\phi = 0.6$ cases show consistent trends in the nearfield with all profiles collapsing at x − x$_0$ < 50 mm. Due to lower heat release, the acceleration in the flame region is not as discernable as in the $\phi = 0.7$ flames. In the farfield, the formation of the central recirculation zones in the open and 20 cm enclosed cases and the acceleration of the flow in the 15.5 cm enclosed cases are still evident. The q'/U$_0$ profiles in Fig. 11b are not as scattered as those shown in Fig. 10b. This is due to the fact that the PIV image degradation due to the weaker flames is not as severe. Again, the features of the q'/U$_0$ profiles are consistent in the near and farfields.

Comparison of the centerline profiles in Fig. 10 and 11 illustrates that the dominant effect of the enclosure on the flame flowfield is manifested in the farfield where a slight decrease in the enclosure size can eliminate the formation of a central recirculation zone. To quantify the downstream effects, the recirculation strengths M$_r$/M$_0$ as functions of axial location were calculated using on the procedure described in Ref [1]. M$_r$ is defined by

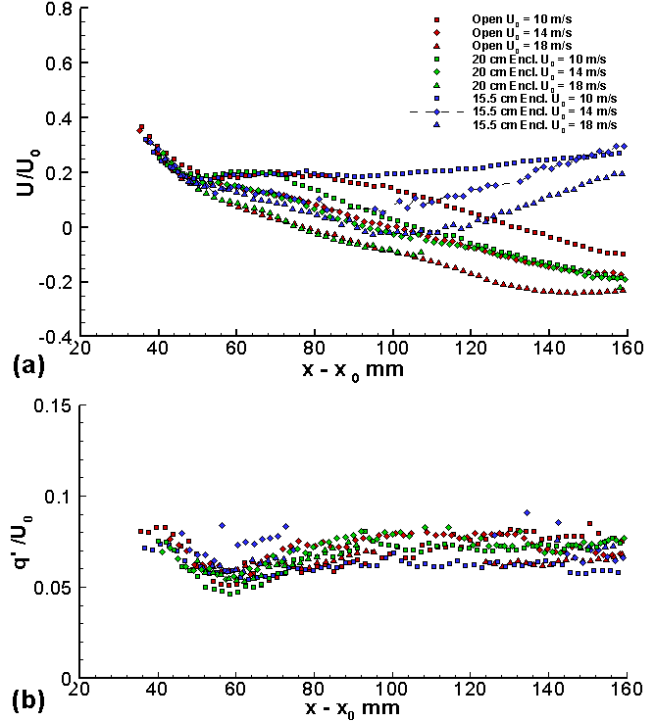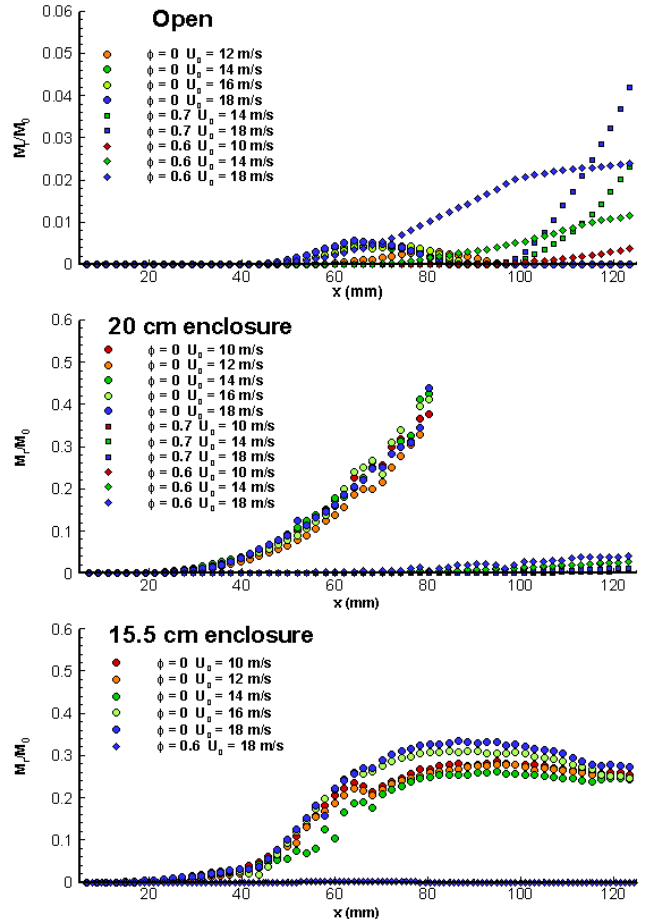$$M_r = \rho \int_0^{R_{U=0}} U(x,r)\pi r\, dr \qquad \text{Eq(3)}$$

Fig 12 Recirculation zone strengths obtained for the open and the enclosed non-reacting flows and CH$_4$/air flames

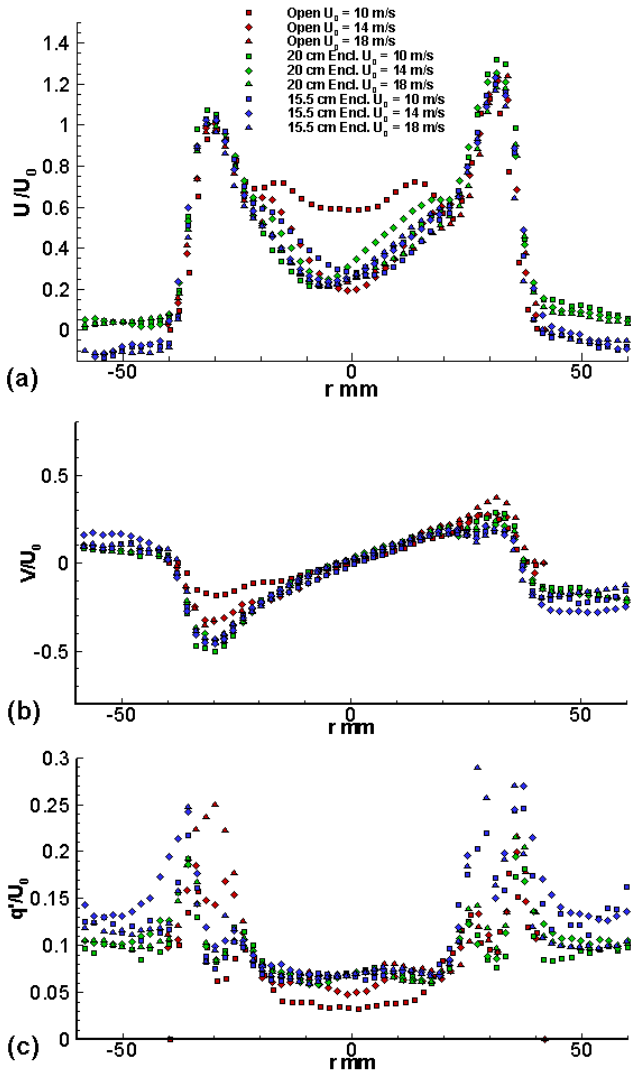Fig 13 Radial profiles for the open and enclosed $\phi = 0.7$ CH$_4$/air flames at x = 6 mm

Fig 14 Radial profiles for the open and enclosed $\phi = 0.6$ CH$_4$/air flames at x = 6 mm

where $R_{U=0}$ is the location of the U=0 contour that outlines the recirculation bubble and ρ is the density of the fluid in the recirculation zone. For the reacting cases, ρ in the recirculation zone was approximated by the adiabatic flame temperature of the reactants without correcting for the radiative heat loss or other cooling effects.

As show in Fig. 12, the plot for the open cases (top) shows that the non-reacting flow recirculation zones are small and weak peaking at a very low value of $M_r/M_0 < 0.01$. Their positions and M_r/M_0 profiles do not change with U_0 and are consistent with self-similarity. The recirculation zones of the $\phi = 0.6$ flames are larger and do not exhibit similarity. Their leading edge shifts upstream with increasing U_0 and the profiles attain M_r/M_0 values of up to 0.03 at the top edge of the PIV domain. The recirculation zones of the $\phi = 0.7$ flames occur farther downstream than the corresponding non-reacting flows and the $\phi = 0.6$ flames. These profiles rise rapidly to
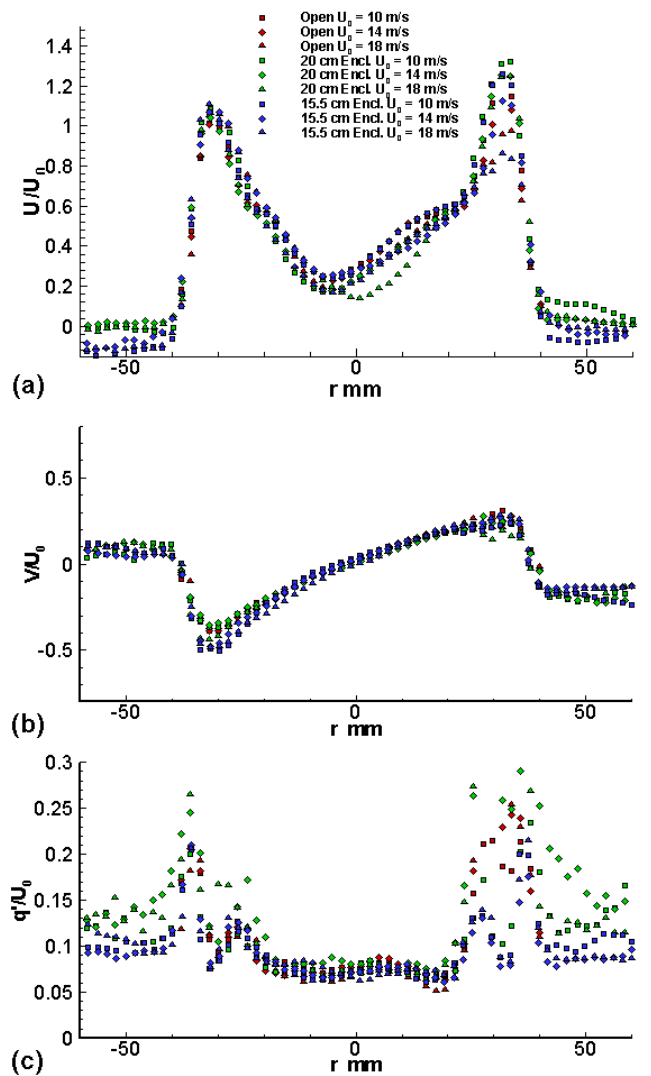
attain high values of $M_r/M_0 = 0.05$. The open flame results shows that the central recirculation zones are affected by the expansion ratio (i.e. ϕ) as well as by the heat release (i.e. U_0).

Fig 12b shows the M_r/M_0 profiles obtained for the 20 cm enclosure. Due to the fact that the non-reacting central recirculation zone boundaries extend beyond the PIV domain (see Fig. 3), calculations of the M_r/M_0 values terminate at positions where the recirculation zone boundaries reach the PIV boundary. The truncated non-reacting M_r/M_0 profiles show that the behavior of the large central recirculation zone is also self-similarity with all the profiles collapsing onto a similar trend. The recirculation zone strength is substantially increased reaching to M_r/M_0 of about 0.4 at the end of the profiles. These values are two orders of magnitude higher than the peak M_r/M_0 values found in the open non-reacting flows. In contrast, the recirculation zone strength for the 20 cm enclosed flames are almost not discernable on Fig 12b that has
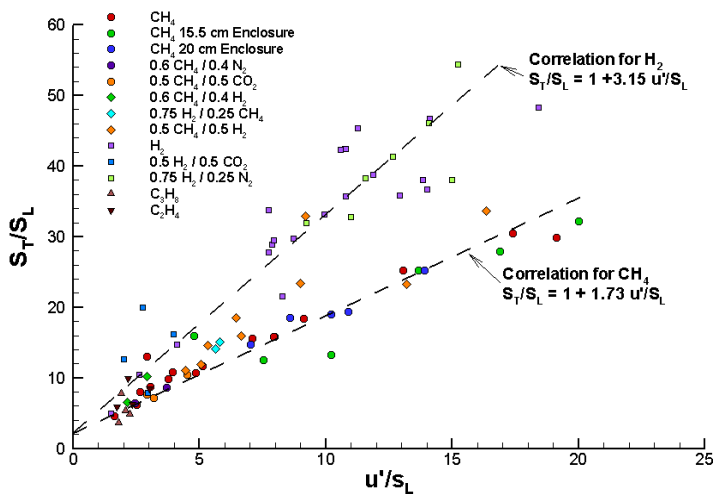
Fig 15 Turbulent flame speeds obtained in open and enclosed LSI flames

a vertical scale ten times larger than in Fig 12a. However, their values are the same as those found in the open flames.

The M_r/M_0 profiles for the 15.5 cm enclosure are shown in Fig 12c. For the non-reacting flows, the M_r/M_0 profiles have relatively flat region following the initial rise. The strength of the recirculation is not as high as in the 20 cm enclosure but their consistent trend shows that they exhibit similarity behavior.

The radial profiles at x = 6.0 mm obtained for the open and enclosed flame flowfields are shown in Figs. 13 and 14. In Fig. 13a, the only profile that deviates from the general trend is the open flame at ϕ = 0.7 and U_0 = 10 m/s. All other U/U_0, V/U_0 and q'/U_0 profiles have consistent trends and distributions that are not different than those shown in Fig. 6 for the non-reacting flows. The same conclusions can be drawn from the profiles of the open and enclosed ϕ = 0.6 flame profiles of Fig. 14.

The analysis of the velocity data obtained from the reacting cases clearly indicates that the nearfield flow structures, in particular the central region where the flame is stabilized by flow divergence, is relatively free of the enclosure effects. To verify that the turbulent flame speeds are not affected by the enclosures, the S_T values for the eighteen open and enclosed flames were deduced and plotted in Fig. 15. This plot differs from previous S_T plots in two significant respects. First of all, it contains S_T data obtained only in the LSI where as previous plots include data from all other low-swirl burners of different sizes and configurations (i.e. air-jet swirler as well as vane swirlers). Second, recent S_L values for un-stretched laminar flames were used for the normalization [19]. The most significant change is the new S_L values at the ultra lean conditions are much higher than the old. Due to this difference, the maximum values of S_T/S_L and u'/S_L for our data set are reduced. However, the adjustment does not change the

linear increasing trend of S_T/S_L with u'/S_L or the correlation constant, K. The value of K for the methane/air flames generated by the LSI is 1.73. This is slightly lower than the value of 2.14 obtained by including the S_T data from all the other low-swirl burners. The correlation constant K for the H_2 flames is the same because only the LSI has been used for H_2 flame studies.

The self-similarity features and linear correlation of S_T with u' show that the analytical model of Eq. 2 also applies to the enclosed flames.

Enclosed H_2 and 0.75 H_2 / 0.25 CH_4 flames

As reported in our previous study of open H_2 flames, high diffusivity and reactivity of H_2 generate phenomena that are not present in hydrocarbon flames. The most significant is the trailing edges of the H_2 or H_2 rich flames curl back upstream and attach to the burner rim when the stoichiometry increases above a certain level. This phenomenon seems to be caused by H_2 diffusing into the lower velocity regions of the outer mixing layer where it is ignited by the trailing edge of the flame. When the flame attaches to the burner rim, it forms an envelope over the reactants. Consequently, the flowfield and the flame/flow dynamics may be affected. The LSI used in this study was configured to address the flame attachment problem. Its swirl number has been lowered to 0.5 and the center channel plate altered to generate a more lifted flame so that flame attachment occurs at a high stoichiometry.

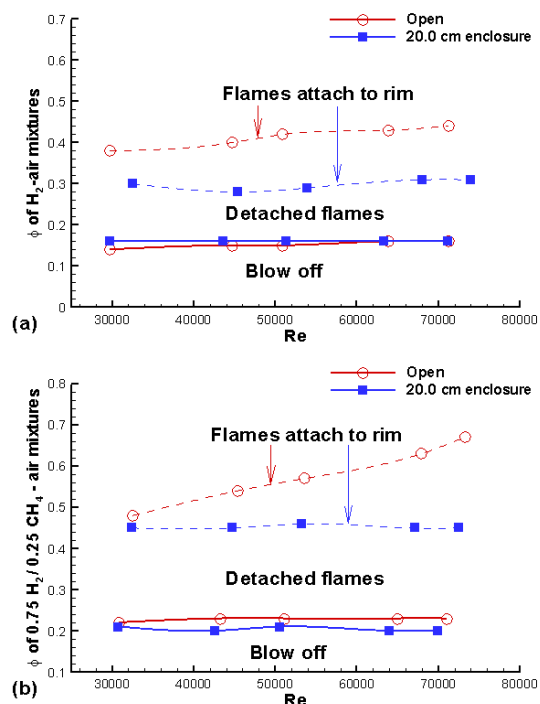Because the attached flame phenomenon originates at the

Fig 16 Lean blow-off and flame attachment limits for H_2 and 0.75 H_2 / 0.25 CH_4 flames
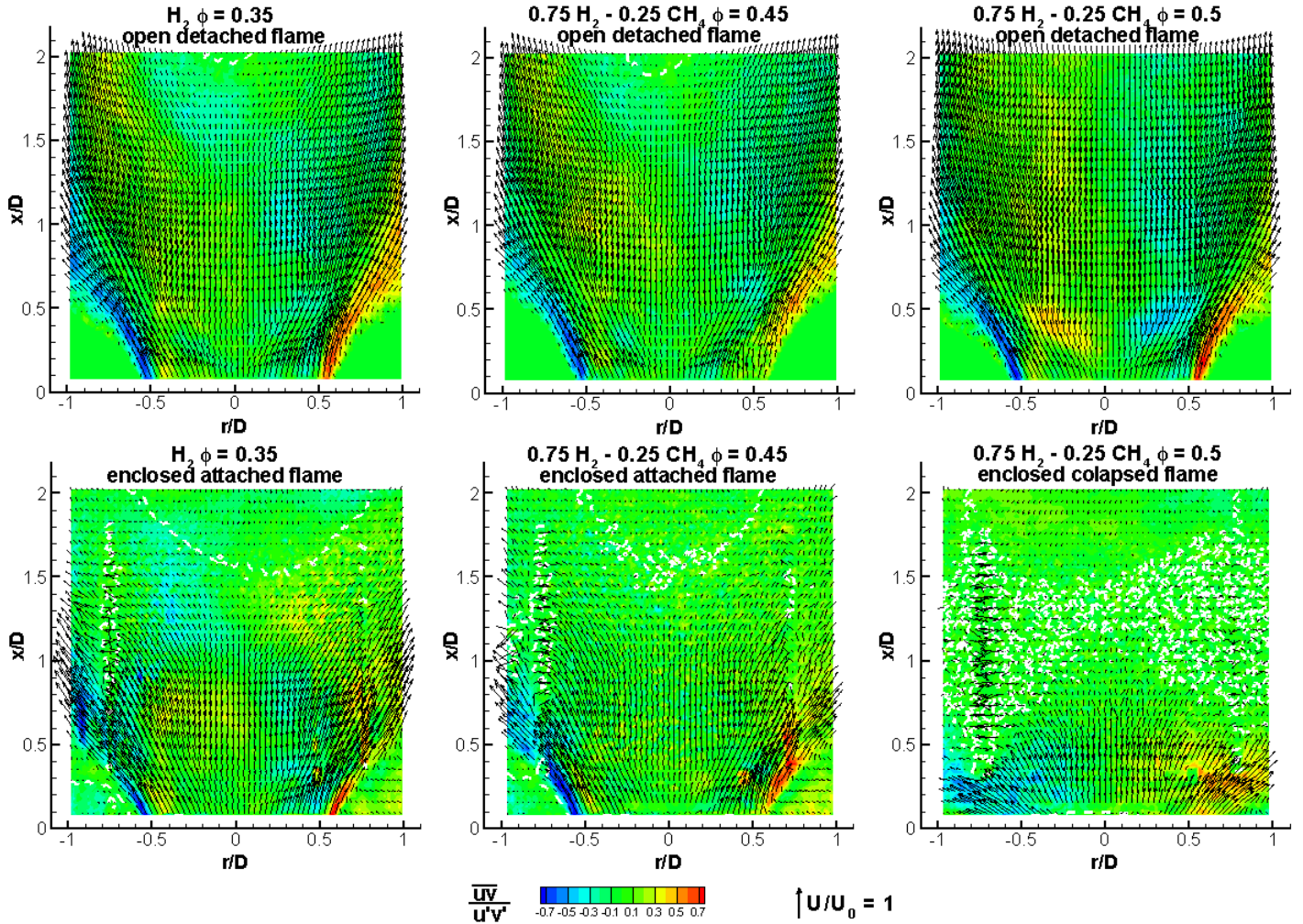
Fig 17 Normalized velocity vectors and Reynolds shear stress of open and enclosed H_2 and 0.75 H_2 / 0.25 CH_4 f;a,es

boundaries of the LSI flow discharge, the dynamics and entrainment in the mixing layer would be the controlling processes. As seen from the results described above, the formation of a robust outer recirculation zone surrounding the mixing layer is one of the significant consequences of the enclosures. Therefore, the formation of the outer recirculation in an enclosure should have a direct effect on the flame attachment phenomenon through its influence on the mixing layer.

Fig. 16 shows the blow-off and flame attachment limits determined for the open and the 20 cm enclosed H_2 and 0.75 H_2 / 0.25 CH_4 flames (Fig 16a) shows that the lean blow-off limit is not sensitive to enclosure effects. Both boundaries are nearly constant with increasing U_0 and are at the same levels. As expected, the enclosure forces the H_2 flames to attach to the rim at lower stoichiometries than in the open (at $\phi \approx 0.3$ compared to $\phi \approx 0.4$). This change can be explained by the outer recirculation zone transporting hot products from the downstream wall regions to promote

ignition and burning within the mixing layers. The blow-off and flame attachment boundaries for the 0.75 H_2 / 0.25 CH_4 flames (Fig. 16b) have the same trends. The only difference is that the attached flame limit for the open cases has a slight increase with Re.

The following conditions were chosen for PIV investigations: H_2-air at $\phi = 0.35$ and $0.75H_2/0.25CH_4$–air at $\phi = 0.45$ and 0.5 at $U_0 = 14$ m/s (Re = 54000) are within the regime bounded by the open and enclosed flame attachment limits. That is, the open flames are fully lifted while the enclosed flames are attached. A significant outcome of these experiments, however, is the discovery of an additional flame phenomenon that is not found in the open. At $\phi = 0.45$, the attached 0.75 H_2 / 0.25 CH_4 flame collapsed from its "M" shape into a very compact almost disk shape flame that covered the LSI exit. The change in flame shape is accompanied by a significant increase in sound levels from the attached flames. However, the sound frequencies do not suggest the onset of low-frequency combustion oscillations.
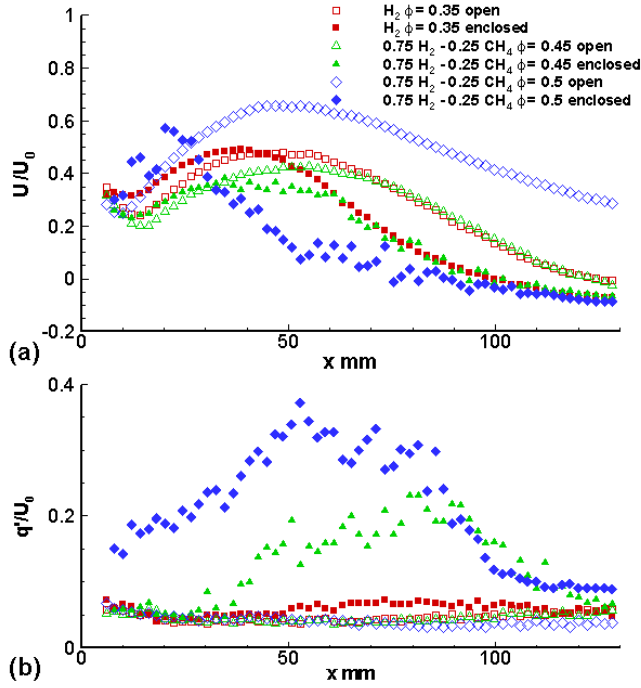
12

Fig. 18 Centerline profiles of open and enclosed H_2 and 0.75 H_2 / 0.25 CH_4 flames

Shown in Fig. 17 are the flowfields of the six open and enclosed H_2 and 0.75 H_2 / 0.25 CH_4 flames. As expected, the flowfield features of the three detached open flames are not significantly different all having the same vector distributions in the nearfield and flow discharge angle. Slight differences are found in the farfield where the formation of weak central recirculation zones is shown on two of the three cases.

For the two attached enclosed flames, the velocity vectors in the central nearfield regions appear to have the same general features as the corresponding lifted flames. The flow discharge angles are larger due to burning in the mixing layer and outside of which is the corner recirculation zone as shown by the velocity vectors near the two lower corners of the PIV domain. In the farfield, the recirculation zones of the enclosed flames are broader and occur closer upstream compared to the open cases.

The formation of the collapsed flame completely changed the flowfield structures. The flow vectors in the nearfield are much faster than those of the attached flames and have very steep discharge angle. This seems to indicate that the flame brush is located at the LSI exit and the nearfield velocity vectors are mostly associated with the products region. As a consequence of the large flow discharge angle, the size of the corner recirculation zone is reduced significantly. In the central region of the PIV domain, degradation due to the high particle deposition is extremely high. Despite these influences, the formation of a broad recirculation can be seen in the farfield.

The axial profiles for the detached, attached and collapsed flames are compared in Fig. 18. Due to the close proximity of these flame brushes to the LSI exit, the values of a_x and x_0
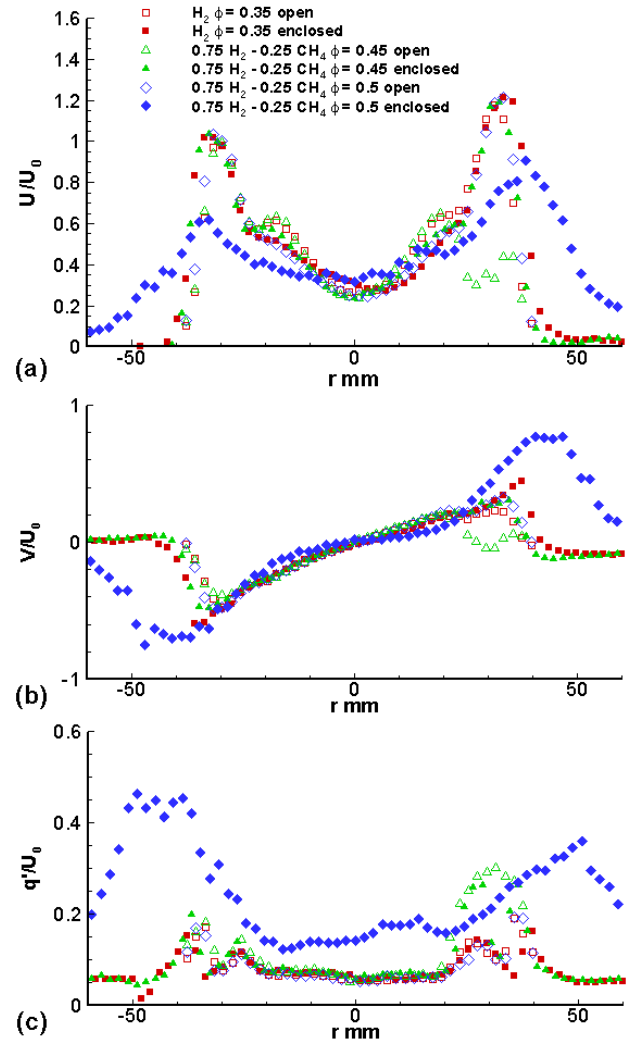

Fig. 19 Radial profiles of open and enclosed H_2 and 0.75 H_2 / 0.25 CH_4 flames at x = 10.0 mm

cannot be deduced reliably from these data and the profiles are plotted as function of x instead of x – x_0. Despite the differences in the flame shapes, many features of the centerline U/U_0 profiles are preserved. The exception is of course the profile of the collapsed flame (0.75 H_2 / 0.25 CH_4 at ϕ = 0.5). Otherwise, typical features such as the nearfield linear decay, flow acceleration due to heat release, and the formation of the weak recirculation zones are all shown.

These results show that the onset of flame attachment does not alter the basic flame stabilization mechanism. Though the flame is attached to the rim, the central divergent region remains the crucial flow feature for stabilizing a stationary propagating flame. A similar conclusion cannot be drawn for the collapsed flame. Through the uncertainties of this set of data are much larger than the other sets, the general shape the U/U_0 profile strongly suggest a different stabilization mechanism. Unfortunately, the PIV can only access the products region of this flame and does not allow us to gain

13

insight into the flow properties in the reactants to investigate this mechanism.

The corresponding q'/U_0 profiles provide more evidence to show that the enclosed attached flames (i.e. H_2 at $\phi = 0.35$ and higher) are not significantly different than the open detached flame. The turbulent kinetic energies in the nearfield ($x < 30$ mm) are at the same level. The rise in q'/U_0 for the enclosed 0.75 H_2 / 0.25 CH_4 flame at $\phi = 0.45$ is due to data degradation associated with particle deposition on the inner surface of the quartz tube. As expected, the q'/U_0 profile of the collapsed flame is different showing very high turbulent kinetic energy in the nearfield.

The radial profiles obtained for the open and enclosed H_2 and 0.75 H_2 / 0.25 CH_4 flames at $x = 10.0$ mm are compared in Fig. 19. These results show again that that nearfield structures are different only for the collapsed enclosed 0.75 H_2 / 0.25 CH_4 flame at $\phi = 0.5$ where the distributions of its U/U_0, V/U_0 and q'/U_0 profiles are inconsistent with the other open and attached flame profiles. In particular, the significant increases in the magnitudes of V/U_0 at $r = -50$ mm and 50 mm accompanied by high q'/U_0 imply a strong coupling of the nearfield flow stricture with the outer recirculation zone. Because the characteristics of the outer recirculation zone are controlled by the configuration of the dump plane, these results show that the H_2 flames are more sensitive to the geometry of the enclosure than the CH_4 flames.

From a practical perspective, configuring a combustor with a sudden expansion dump plane has no direct benefit. It is employed here to facilitate experimental measurements because any other dump plane configurations would have blocked laser access to the nearfield region. Eliminating the outer recirculation zone and its influence on the flame is feasible. It is already a standard practice for the industrial low-swirl burners manufactured by Maxon Corporation. They all feature a divergent cone attached to the burner exit to guide the flow transition from the burner to the combustor casing. This design has proven to be effective in sustaining stable flames and to help in reducing flame noise associated with the flame being intermittently entrained into the outer recirculation zone. The use of a guide cone may provide a simple remedy to address the H_2 flame attachment problem. This aspect is being investigated in the laboratory.

CONCLUSIONS

Particle Image Velocimetry (PIV) was used to investigate the effects of enclosure on the flame and flowfield properties of a developmental low-swirl injector (LSI) of 6.35 cm diameter configured for burning of hydrocarbon and hydrogen fuels in gas turbines. The experiments were performed at atmospheric conditions. The velocity data were analyzed to obtain the parameters in an analytical model that encapsulates the basic LSI flame stabilization mechanism.

Two quartz cylinders of 35 cm in length were used to simulate the combustor casing of a gas turbine. The 20 cm

diameter cylinder gives an enclosure to LSI diameter ratio of 3.14:1 that is close to the optimum 3:1 ratio prescribed for industrial low-swirl burners. The smaller 15.5 cm quartz cylinder (2.44:1 diameter ratio) was chosen to study the enclosure size effects. The experiments consisted of a set of baseline data for the open and enclosed non-reacting flows at five bulk flow velocities between $10 < U_0 < 18$ m/s. The CH_4 air flames were invested in the open and in the two enclosures at $\phi = 0.6$ and 0.7 and at $U_0 = 10$, 14, and 18 m/s. The H_2 and 0.75 H_2 / 0.25 CH_4 flames were studied in the open and in the 20 cm quartz cylinder at $U_0 = 10$, 14, and 18 m/s and at various stoichiometries.

The results show that the enclosures have significant effects on the non-reacting flowfield. Most prominent is the enlargement and strengthening of the central recirculation zone. Calculation of the recirculation strength showed an increase of more than an order of magnitude compared to the open flows. Features of the non-reacting flowfields within the two enclosures are the same. Both have high nearfield divergence rates and their axial and radial velocity distributions exhibit self-similarity features that are different than those of the open non-reacting flows.

In contrast, the flowfields of the open and enclosed CH_4 flames show very little enclosure effects. There are insignificant differences in their normalized divergence rates, the virtual origins and the turbulent flame speeds. Therefore, the flames within these enclosures are stabilized by the divergent flow supplied through the LSI nozzle despite the fact that strong outer recirculation zones are formed at the corner of the dump plane. In the farfield, weak central recirculation zones formed in the open and the 20 cm enclosed flames. They are similar in size and strength. Flames within the smaller 15.5 cm enclosure do not generate central flow recirculation illustrating that the enclosure effects are manifested in the farfields of the CH_4 flames and in the corners of the dump plane.

The experiments on the H_2 and 0.75 H_2 / 0.25 CH_4 flames enclosed by the 20 cm cylinder showed that the outer recirculation zone generated at the corner of the sudden expansion dump plane promotes flame attachment. That is, the trailing edge of the enclosed LSI flame attaches to the rim at lower stoichiometry than in the open. However, the properties and nearfield flow features of the attached flames are similar to those of the lifted flames. At higher stoichiometries, the attached flame collapses to form a compact disc-shaped flame that has very different flowfield structures. These results show that the enclosure effects on the LSI are strongly coupled to the fuel type and the combustor geometry.

For highly diffusive fuels such as H_2, the outer-recirculation zone formed in the corners of combustor dump plane provides an additional flame stabilization mechanism. Therefore, the elimination of the outer recirculation zone by the use of a. divergent cone at the LSI nozzle discharge seems to be a necessary component for the LSI H_2 combustor. The

integration of the divergent cone into the design of the LSI is in progress.

The velocity data and the experimental observations on the enclosure effects reported here provide the basis for validating the results from computational fluid mechanics. Improving the fidelity of the computational methods so that they predict correctly the changes in the enclosed non-reacting and reacting flowfields is essential for the development of the CFD methods as design tools for LSI adaptation to fuel flexible H_2 turbines.

ACKNOWLEDGMENTS

REFERENCES

1. Johnson, M.R., D. Littlejohn, W.A. Nazeer, K.O. Smith, and R.K. Cheng, *A Comparison of the Flowfields and Emissions of High-swirl Injectors and Low-swirl Injectors for Lean Premixed Gas Turbines.* Proc. Comb. Inst, 2005. **30**: p. 2867 - 2874.
2. Nazeer, W.A., K.O. Smith, P. Sheppard, R.K. Cheng, and D. Littlejohn. *Full Scale Testing of a Low Swirl Fuel Injector Concept for Ultra-Low NOx Gas Turbine Combustion Systems*. in *ASME Turbo Expo 2006: Power for Land, Sean and Air*. 2006. Barcelona, Spain: ASME.
3. Cheng, R.K. and D. Littlejohn, *Laboratory Study of Premixed H2-Air & H2-N2-Air Flames in a Low-swirl Injector for Ultra-Low Emissions Gas Turbines.* Journal of Engineering for Gas Turbines and Power, 2008. **In press**. also ASME GT2007-27512.
4. Yegian, D.T. and R.K. Cheng, *Development of a Lean Premixed Low-Siwlr Burner for Low NOx Pracital Applications.* Comb. Sci. Tech., 1998. **139**: p. 207-227.
5. Chan, C.K., K.S. Lau, W.K. Chin, and R.K. Cheng, *Freely Propagating Open Premixed Turbulent Flames Stabilized by Swirl.* Proc. Comb. Inst., 1992. **24**: p. 511-518.
6. Cheng, R.K., D.T. Yegian, M.M. Miyasato, G.S. Samuelsen, R. Pellizzari, P. Loftus, and C. Benson, *Scaling and Development of Low-Swirl Burners for Low-Emission Furnaces and Boilers.* Proc. Comb. Inst., 2000. **28**: p. 1305-1313.
7. Bedat, B. and R.K. Cheng, *Experimental Study of Premixed Flames in Intense Isotropic Turbulence.* Combustion and Flame, 1995. **100**(3): p. 485-494.
8. Cheng, R.K., *Velocity and Scalar Characteristics of Premixed Turbulent Flames Stabilized By Weak Swirl.* Combustion and Flame, 1995. **101**(1-2): p. 1-14.
9. Plessing, T., C. Kortschik, M.S. Mansour, N. Peters, and R.K. Cheng, *Measurement of the Turbulent Burning Velocity and the Structure of Premixed Flames on a Low Swirl Burner.* Proc. Comb. Inst., 2000. **28**: p. 359-366.
10. Shepherd, I.G. and R.K. Cheng, *The burning rate of premixed flames in moderate and intense turbulence.* Combustion and Flame, 2001. **127**(3): p. 2066-2075.
11. Cheng, R.K., I.G. Shepherd, B. Bedat, and L. Talbot, *Premixed turbulent flame structures in moderate and intense isotropic turbulence.* Combustion Science and Technology, 2002. **174**(1): p. 29-59.
12. Bell, J.B., M.S. Day, I.G. Shepherd, M.R. Johnson, R.K. Cheng, J.F. Grcar, V.E. Beckner, and M.J. Lijewski, *Numerical Simulation of a Laboratory-Scale Turbulent V-Flame.* Proc. Natl. Academy Sci. USA, 2005. **102**(29): p. 10006-10011.
13. Littlejohn, D. and R.K. Cheng, *Fuel Effects on a Low-swirl Injector for Lean Premixed Gas Turbines.* Proc. Comb. Inst., 2007. **31**(2): p. 3155-3162.
14. Cheng, R.K., D. Littlejohn, W.A. Nazeer, and K.O. Smith, *Laboratory Studies of the Flow Field Characteristics of Low-Swirl Injectors for Application to Fuel-Flexible Turbines.* Journal of Engineering for Gas Turbines and Power, 2008. **130**(2): p. 21501-21511.
15. Mellings, A., *Tracer particles and seeding for particle image velocimetry.* Measurements Sci. & Tech., 1997. **8**: p. 1406-1416.
16. Wernet, M.P. *'Fuzzy logic enhanced digital PIV processing software',.* in *18th International Congress on Instrumentation for Aerospace Simulation Facilities*. 1999. Toulouse, France.
17. Lilley, D.G., *Swirl Flows in Combustion : A Review.* AIAA Journal, 1977. **15**(8): p. 1063-1078.
18. Cheng, R.K., D. Littlejohn, W.A. Nazeer, and K.O. Smith. *Laboratory Studies of the FLowfield Characteristics of Low-siwrl Injectors for Adaptation to Fuel-Flexible Turbines*. in *ASME Turbo Expo 2006: Power for Land Sea and Air*. 2006. Barcelona, Spain: ASME.
19. Jomaas, G., X.L. Zheng, D.L. Zhu, and C.K. Law, *Experimental determination of counterflow ignition temperatures and laminar flame speeds of C2-C3 hydrocarbons at atmospheric and elevated pressures.* Proceedings of the Combustion Institute, 2005. **30**(1): p. 193-200.